Phase oscillators in modular networks: The effect of nonlocal coupling

Sangeeta Rani Ujjwal,[1] Nirmal Punetha,[2] and Ramakrishna Ramaswamy[1]

[1]*School of Physical Sciences, Jawaharlal Nehru University, New Delhi 110 067, India*

[2]*Department of Physics and Astrophysics, University of Delhi, Delhi 110 007, India*

We study the dynamics of nonlocally coupled phase oscillators in a modular network. The interactions include a phase lag, α. Depending on the various parameters the system exhibits a number of different dynamical states. In addition to global synchrony there can also be *modular synchrony* when each module can synchronize separately to a different frequency. There can also be *multicluster frequency chimeras*, namely coherent domains consisting of modules that are separately synchronized to different frequencies, coexisting with modules within which the dynamics is desynchronized. We apply the Ott-Antonsen ansatz in order to reduce the effective dimensionality and thereby carry out a detailed analysis of the different dynamical states.

I. INTRODUCTION

The synchronization properties of oscillators on complex networks have long been of interest due to applications in diverse branches of physics [1,2], chemistry [3,4], and biology [2,5]. A class of complex networks that have recently attracted considerable attention are those with a modular structure, namely with groups of nodes that have significantly more links connecting members of the group (or module) and with fewer links between modules. Modular networks thus have a "community" structure, with distinct patterns of internal and external connectivity [6], and this has a significant impact on the process of synchronization of dynamical systems connected in such a topology. Systems on nodes belonging to the same module or community synchronize with greater probability for lower coupling [7,8] compared to systems on nodes in different communities.

In this paper we consider phase oscillators on modular networks and examine the effect of *nonlocal* coupling. Although collective dynamics has been extensively studied in networks of locally or globally coupled oscillators [9–12], a study of the effects of nonlocal coupling is interesting since in general most interactions are neither purely local or purely global; they have a finite range that depends on the model as well as the network topology [13–15]. Nonlocal coupling, although relatively less explored [16], is of considerable current interest following the observations by Kuramoto and coworkers [17] that such coupling in an ensemble of symmetrically and identically coupled dynamical systems can give rise to complex spatiotemporal dynamics, the so-called *chimera* states [18]. Chimeras are dynamically segregated states, with some of the oscillators synchronizing in a coherent cluster (or clusters), while others resist synchronization and remain in an incoherent state. Such a state is dynamically unexpected, and attempts have been made over the past few years to understand the origin of such states [17–20], given that there are possible applications to phenomena such as unihemispheric sleep in mammals [21], bump states in neural networks [22], power grids [23,24], etc. Chimera states have been shown to arise in a number of experiments [25–28] and in an increasing range of theoretical studies [29–32].

In the present work, we consider a modular network of phase oscillators and study the different synchronization patterns that emerge when the coupling has both local and nonlocal components. The intermodular nonlocal coupling is taken to have a piecewise linear dependence, similar to that considered in our earlier work [33]. In addition to global synchronization (GS) where all oscillators lock to a common frequency, we find states where all oscillators within a module synchronize separately to different frequencies: The network shows modular synchronization (MS). In addition to MS, the network can also exhibit a chimeric state where some modules are synchronized to distinct frequencies, while other clusters are desynchronized. We term these states multicluster frequency chimeras (MFC) since they differ considerably from the types of chimeric states observed in earlier studies that have considered nonlocal coupling in modular networks [34,35].

The model dynamical system and network is described in the following section. Some analysis of the nature of the states and their stabilities is possible, and this is presented, along with numerical results, in Sec. III. The different dynamical scenarios are discussed in some detail in Sec. III as well. We then carry out a dimensionality reduction via the Ott and Antonsen ansatz [36]. The number of equations reduces to the number of modules, and this permits further analysis and validation of our numerical results. We conclude with a summary and a discussion of the main results in Sec. IV.

II. MODEL DESCRIPTION

We consider a simple modular network of phase oscillators, with M modules, each of which has an equal number n of nodes. The size of the system is thus $N = nM$. The coupling between the oscillators is symmetric and is such that oscillators in the same module interact with a constant coupling, while oscillators in different modules interact through a nonlocal coupling that decays with the "distance" between the modules. A schematic diagram of such network is shown in Fig. 1. The dynamics of the oscillators in the network is given by

$$\frac{\partial \phi_i^a}{\partial t} = \omega + \frac{1}{N} \sum_j{}' G^{ab} \sin\left(\phi_j^b - \phi_i^a - \alpha\right), \qquad (1)$$

where the summation is over all oscillators in the network, while the prime on the sum indicates that the self-interaction term is absent. In Eq. (1), the notation is as follows: The
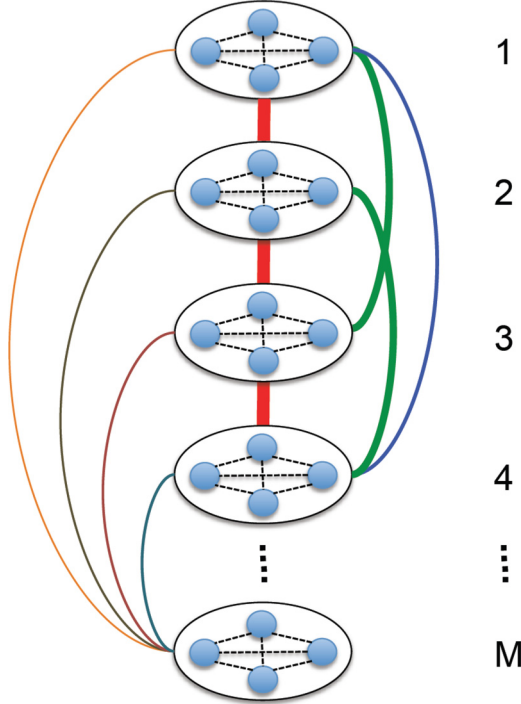
FIG. 1. Schematic diagram of a nonlocally coupled modular network. The intramodular connections are shown by dashed lines while the connections between different modules are shown by solid lines. The thickness of the solid lines represents the strength of the connection, the adjacent modules are strongly connected but coupling strength decreases as the distance between the modules increases.

superscripts a,b are the module indices, while the subscript indexes the different oscillators in a module. Thus ϕ_i^a is the phase of the ith oscillator in the ath module, $i = 1,2,\ldots,n$, and $a = 1,2,\ldots,M$. The natural frequency of the oscillators is denoted by ω, since all the oscillators are identical, we can put $\omega = 0$ without loss of generality. The interactions in the network include a phase lag, namely the parameter $\alpha \in (0, \frac{\pi}{2})$. The coupling G^{ab} is defined as follows:

$$G^{ab} = \begin{cases} \frac{\varepsilon(M-|a-b|)}{M^2}, & \text{if } a \neq b \\ \mu, & \text{if } a = b \end{cases}, \qquad (2)$$

where $a,b = 1,\ldots,M$ are the module indices. The maximum value of the nonlocal coupling, $G_{\max}$ is attained when the interaction is considered between adjacent modules ($|a - b| = 1$), and this coupling decreases linearly with the difference in the module indices. Note that the function is non-negative and is normalized to have unit integral. The intra-modular connections are taken to be of equal strength μ.

We study the synchronization properties of the system as a function of phase lag parameter, α. The existence of a lag makes nodes that are coupled to each other maintain a finite phase difference and thus this parameter plays a major role in balancing the degree of synchrony and asynchrony in the network. As the value of α is varied the system shows different scenarios of synchronization, and these are discussed in the following section.
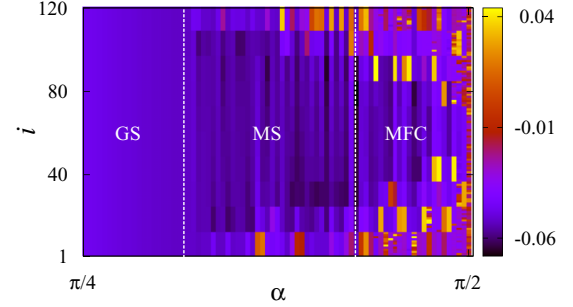

FIG. 2. Oscillator frequencies as a function of the phase lag parameter, α, for $M = 10$, $N = 120$, and $\mu = 0.1$. In the region of global synchronization (GS) all oscillators have the same frequency; in modular synchronization (MS) and multicluster frequency chimeras (MFC), different groups of oscillators have distinct frequencies.

III. RESULTS

We first present some numerical results for a system with $n = 12$ oscillators in $M = 10$ modules, taking the intramodule coupling strength parameter $\mu = 0.1$ and the intermodule parameter $\varepsilon = 1.0$. In simulations the initial phases are taken randomly between 0 and 2π. Fig. 2 summarizes the typical behavior of the network of 120 oscillators when the phase lag parameter α is varied from 0 to $\pi/2$. The distinct states that are apparent can be described as follows:

(1) For small α, a global synchronized state (GS) is observed. All oscillators in the network lock on to a common frequency. Oscillators in the same module have the same phase, and there is a phase-lag between the different modules.

(2) For somewhat higher values of α, MS is seen. Each module synchronizes to a *different* frequency.

(3) When α is further increased, some of the modules become desynchronized, and MFCs are formed. Synchronized modules coexist with desynchronized modules. However, a given module is either completely synchronized or completely desynchronized; chimeras do not exist *within* a module.

(4) For α near $\pi/2$, the system is completely desynchronized.

These results are typical: the same set of states are found to occur as a function of α, regardless of the numbers of modules or oscillators and even when the numbers of oscillators in different modules are not identical. It is therefore useful to define a measure of the dynamical diversity of the network for a given α through the number N_f of *distinct* frequencies in the system. This number varies between 1 when all oscillators are in synchrony and N when each oscillator has a different frequency. The ratio

$$\gamma = \frac{N_f}{M} \qquad (3)$$

thus functions as an order parameter. In GS the system has a single frequency, $N_f = 1$. In the MS state each module has a different synchronized frequency and $N_f = M$, while in the MFC, $N_f > M$. Thus $\gamma < 1$ for GS, $\gamma = 1$ for MS, and $\gamma > 1$ for MFC. The numerical frequency as a function of α for a typical case is plotted in Fig. 3(a), and the variation of γ with
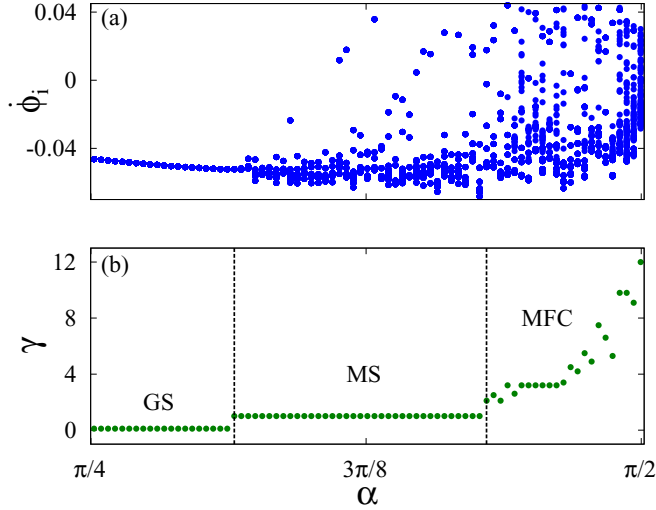
FIG. 3. Frequencies of the oscillators in the network as a function of α. The parameter γ [see Eq. (3)] is computed from the number of distinct frequencies, N_f, and is shown as a function of α.

α is shown in Fig. 3(b) for comparison. A detailed description of these states is given in the following sections.

A. Globally synchronized states

For small α the system of Eq. (1) becomes globally synchronized. All oscillators lock to a common synchronized frequency, but the phase distribution is such that oscillators in the same module have identical phases while there is a phase lag between oscillators in different modules. A typical phase snapshot of such a GS network with $M = 10, n = 12, \mu = 0.1$, and $\alpha = 0.1$ is shown in Fig. 4. Since all the oscillators in the same module have the same phase, each module in the network can be characterized by a modular phase δ^a with reference to the first module, δ^1. The distribution of modular phases, δ^a, for different numbers of modules, M (keeping N fixed), is plotted in Fig. 5 and as can be seen the distribution of δ^a is symmetric about the central module in the network, i.e., $\delta^k = \delta^{M-(k-1)}$.
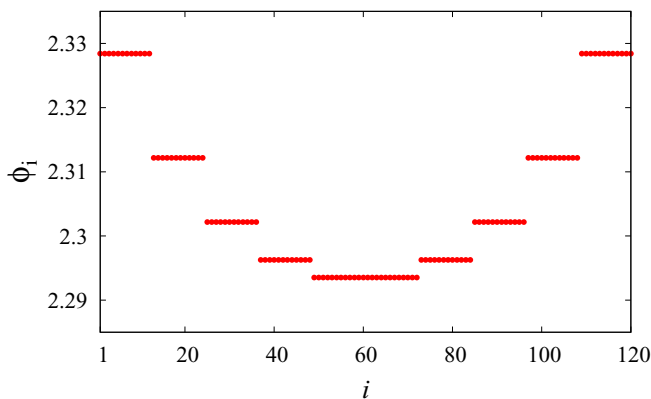

FIG. 4. Phase snapshot of the oscillators in the global synchronized (GS) state at $\alpha = 0.1$, for a network of $N = 120$ oscillators in $M = 10$ modules.
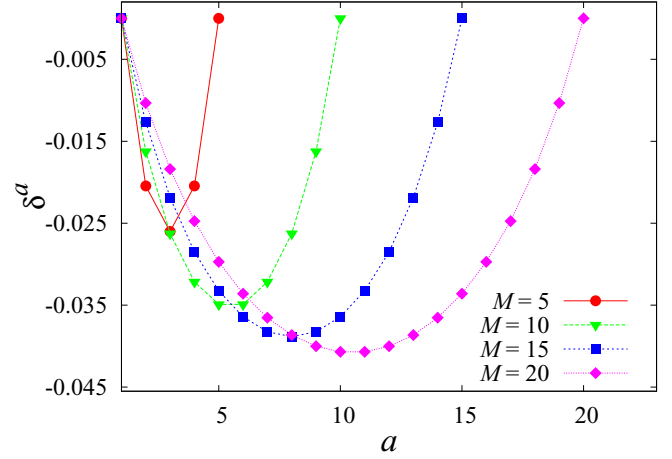

FIG. 5. Phase of a th module, δ^a with respect to first module, δ^1 plotted for different numbers of modules M.

In this regime, Eq. (1) can be solved analytically to obtain the expression for synchronized frequency, Ω. Combining the intramodular coupling μ and nonlocal coupling function to form a weighted connection matrix, $\mathbf{W}$, the equation of motion for the ith oscillator can be written as:

$$\frac{\partial \phi_i}{\partial t} = \frac{1}{N} \sum_{j=1}^{N} W_{ij} \sin(\phi_j - \phi_i - \alpha). \qquad (4)$$

Here W_{ij} are the elements of the $N \times N$ weighted matrix $\mathbf{W}$, written in block form as

$$\mathbf{W} = \begin{bmatrix} \mu\mathbf{E} & G^{12}\mathbf{F} & G^{13}\mathbf{F} & \dots & G^{1M}\mathbf{F} \\ G^{21}\mathbf{F} & \mu\mathbf{E} & G^{23}\mathbf{F} & \dots & G^{2M}\mathbf{F} \\ G^{31}\mathbf{F} & G^{32}\mathbf{F} & \mu\mathbf{E} & \dots & G^{3M}\mathbf{F} \\ \vdots & \vdots & \vdots & \ddots & \vdots \\ G^{M1}\mathbf{F} & G^{M2}\mathbf{F} & G^{M3}\mathbf{F} & \dots & \mu\mathbf{E} \end{bmatrix}, \qquad (5)$$

where $\mathbf{E}$ is a $(n \times n)$ matrix with diagonal and off-diagonal entries being zero and 1, respectively. $\mathbf{F}$ is also a matrix of size $n \times n$, with all entries equal to unity. Expanding the coupling term in Eq. (4) gives

$$\frac{\partial \phi_i}{\partial t} = \frac{1}{N} \sum_{j=1}^{N} W_{ij}[\cos\alpha \sin(\phi_j - \phi_i) - \sin\alpha \cos(\phi_j - \phi_i)]. \qquad (6)$$

For synchronized solutions,

$$\phi_i = \Omega t + \delta_i, \qquad (7)$$

where Ω is the collective frequency of the oscillators and δ_i's are the respective phases, with respect to the first oscillator, namely δ_1, which we set to zero. Putting this solution in Eq. (6) gives

$$\Omega = \frac{1}{N} \sum_{j=1}^{N} W_{ij}[\cos\alpha \sin(\delta_j - \delta_i) - \sin\alpha \cos(\delta_j - \delta_i)]. \qquad (8)$$

When averaged over all the oscillators, the first term in the expansion vanishes and the equation reduces to

$$\Omega = -\frac{\sin\alpha}{N^2} \sum_{i=1}^{N} \sum_{j=1}^{N} W_{ij} \cos(\delta_j - \delta_i). \qquad (9)$$

Introducing the notation $\Delta_{ij} = \delta_j - \delta_i$, the above equation reads

$$\Omega = -\frac{\sin\alpha}{N^2} \sum_{i,j} W_{ij} \cos\Delta_{ij}. \qquad (10)$$

For $M = 2$ an exact solution to Eq. (4) can be obtained for the in-phase synchronization state, $\Delta_{ij} = 0, \forall i,j; i,j = 1,2,\dots,N$. The common frequency Ω is given by

$$\Omega = -\frac{\sin\alpha}{N^2} \sum_{i,j} W_{ij}. \qquad (11)$$

For higher M, obtaining an exact solution for Ω and the $\delta_i's$ is nontrivial, but it is possible to obtain an estimate for Ω by expanding the right-hand side of Eq. (9) and retaining terms up to second order in Δ,

$$\Omega = -\frac{\sin\alpha}{N^2} \sum_{i,j} W_{ij} \left[1 - \frac{\Delta_{ij}^2}{2} + \cdots \right]. \qquad (12)$$

Rearrangement gives

$$\Omega = -\frac{\sin\alpha}{N^2} \sum_{i,j} W_{ij} + \frac{\sin\alpha}{2N^2} \sum_{i,j} W_{ij}\Delta_{ij}^2, \qquad (13)$$

for which a mean-field approximation is

$$\Omega = -\frac{\sin\alpha}{N} \langle W \rangle + \frac{\sin\alpha}{2N} \langle W\Delta^2 \rangle, \qquad (14)$$

$\langle \rangle$ being an average over all oscillators, and

$$\langle W \rangle = \frac{1}{N} \sum_{i,j} W_{i,j} \quad \text{and} \quad \langle W\Delta^2 \rangle = \frac{1}{N} \sum_{i,j} W_{i,j}\Delta_{ij}^2. \quad (15)$$

The first term on the right-hand side of Eq. (14) depends on the network topology, while the latter one depends on the phase differences, and it can be seen that the collective frequency has a dependence on the phase differences, making any solution fairly nontrivial. However, considering terms that are independent of the δ's gives a good estimation of the synchronized frequency Ω as a function of α. The analytical estimate for Ω obtained from Eq. (14) is plotted in Fig. 6 along with the values obtained numerically for different M. The numerical frequencies (shown in blue circles) match well with the analytical values (shown by a red dashed line) in the GS region. For fixed M, Ω decays with α, linearly for small values of α. As higher-order terms begin to play a role, the approximation worsens, and there is a clear deviation from linearity. As α increases further the system is no longer in a synchronized state, as indicated by the scattered values of numerical frequencies (blue circles).

Kori and Mikhailov [16] have noted, in a study of an ensemble of phase oscillators that share some of the features of the present modular network, that the entrainment frequency window decreases with an increase in the network depth [16]. This quantity, in our present situation, would roughly
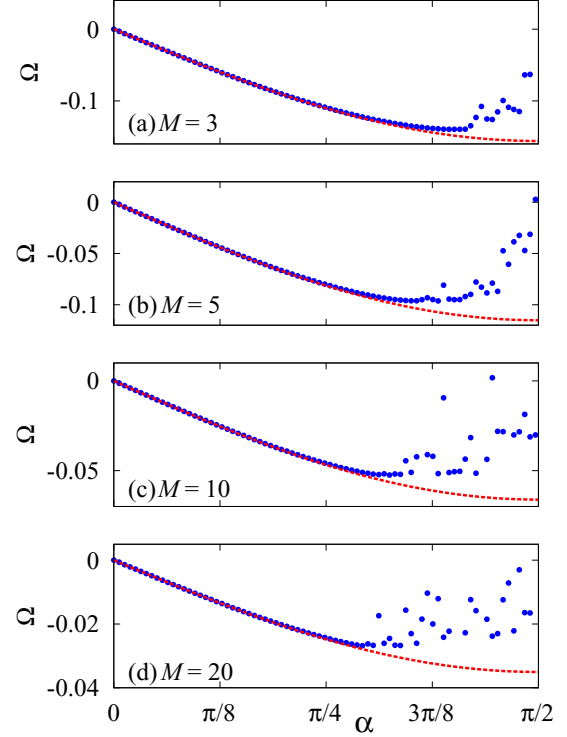

FIG. 6. Comparison of synchronized frequency, Ω obtained analytically (the red dashed line) and numerically (blue circles) as a function of α for different numbers of modules in the network: (a) $M = 3$, (b) $M = 5$, (c) $M = 10$, (d) $M = 20$.

be proportional to the number of modules. A similar effect can be seen in Fig. 6 where analytical and numerical values of Ω are compared as a function of α for different M. Note that as the number of modules M increases, the value of α above which a synchronized state ceases to exist shifts towards lower values and the synchronized region narrows as well.

The stability of the GS state can be analyzed in the usual manner. Assuming that $\Phi_P^a(t)$ is a periodic solution of period $T = 2\pi/\Omega$ for the ath module when there is GS, then one can see that the synchronized solutions satisfy

$$\frac{\partial \Phi_P^a}{\partial t} = -\frac{(n-1)\mu}{N} \sin\alpha + \frac{1}{M} \sum_{b}' G^{ab} \sin\left(\Phi_P^b - \Phi_P^a - \alpha\right), \qquad (16)$$

where $a,b = 1,\dots,M$, and the prime on the summation indicates that $b \neq a$. To each module we apply perturbations ξ^a transverse to the synchronized periodic solution of all oscillators, namely

$$\phi^a(t) = \Phi_P^a(t) + \xi^a(t), \qquad (17)$$

and by substituting these in Eq. (16), one obtains the linearized variational equation,

$$\frac{\partial \xi^a}{\partial t} = \frac{1}{M} \sum_{b}' G^{ab} \cos\left(\Phi_P^b - \Phi_P^a - \alpha\right)(\xi^b - \xi^a). \qquad (18)$$

The stability of the GS state thus does not depend on the intramodular coupling strength μ, since these terms are excluded from the variational equation ($b = a$ is not allowed). To check the stability of GS state, we calculate Floquet

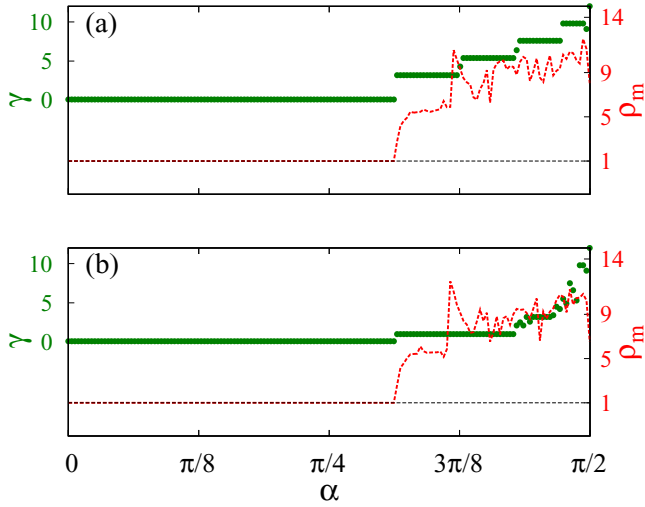FIG. 7. The parameter γ (green circles) and the largest Floquet multiplier, ρ_m (red dashed line) as a function of α showing the stability of the GS state for (a) $\mu = 0$ and (b) $\mu = 0.1$.

FIG. 8. (a) Phase and (b) frequency snapshots of the oscillators in the modular synchronized (MS) state for $\alpha = 1.32$ and $M = 10$.

multipliers for synchronized periodic orbit of time period $T = 2\pi/\Omega$. The largest real part of the Floquet multiplier ρ_m (calculated for 100 initial conditions) is plotted along with the order parameter γ in Fig. 7. The region where synchronized solutions Eq. (7) are stable are those for which magnitude of ρ_m is less than unity. The Goldstone mode corresponds to the trivial multiplier $\rho = 1$ and relates to perturbations along the direction of the periodic orbit. Above $\alpha \approx 1.0$, the magnitude of ρ_m becomes greater than unity, indicating that the GS state is unstable. The cases of $\mu = 0$ and $\mu = 0.1$ are shown in Fig. 7.

B. Modular synchronization

For intermediate values of α the system shows different behaviors, depending upon the strength of the intramodular coupling μ. So long as $\mu \neq 0$, the system can exhibit MS where oscillators within a module are in complete synchrony but the frequency varies from module to module. Unlike the case of GS, in MS the oscillators from each module lock to a distinct time-dependent frequency which differs for each module. Phase and frequency snapshots of the system in the MS state are shown in Fig. 8: In this case the network has M distinct frequencies and thus the order parameter $\gamma = 1$.

We find that MS occurs only when $\mu \neq 0$. When there is no intramodular coupling, oscillators within a given module are unable to synchronize among themselves, so one can observe GS and MFC but there can be no MS. In Fig. 9 the variation of γ as a function of α is plotted for different values of μ. The absence of MS for $\mu = 0$, namely for a purely multipartite network, can be seen in Fig. 9(a).

For higher values of μ the system shows MS and indeed the region of MS increases with increasing μ (Fig. 9). These findings seem to suggest that intramodular connectivity is necessary to observe MS in such networks. We also note that the value of α at which system makes a transition from GS to MS (for $\mu > 0$) or MFC (for $\mu = 0$) is independent of the value of μ. This is evident from the Eq. (18) obtained for the
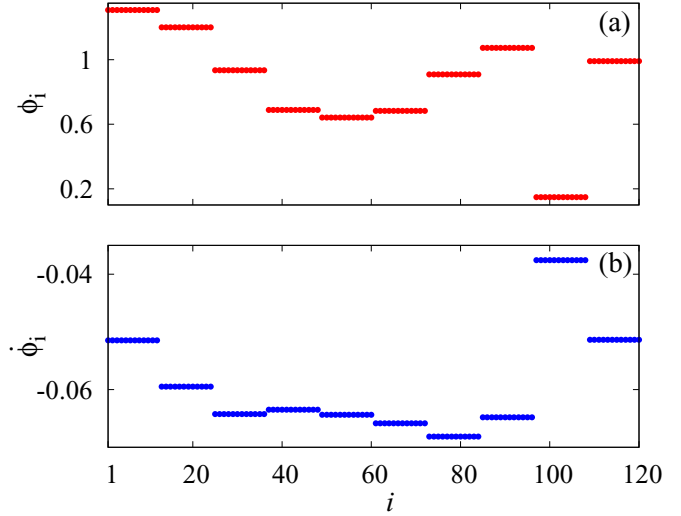
stability of the GS state where the intramodular coupling do not affects the stability of GS state. We therefore infer that the number of modules M determines the region of GS, while the intramodular coupling strength μ decides the region of MS as a function of α.

C. Multicluster frequency chimeras

For higher α, chimeric states occur in the modular network. In some modules the dynamics are synchronized while in others the oscillators evolve incoherently. In each coherent module, the frequency of synchronized motion is distinct, and thus we term this kind of chimeric state a MFC. The MFCs should by distinguished from the frequency chimera states that are observed in globally coupled Stuart-Landau oscillators [37]; there all oscillators that form a part of the coherent group have a single frequency. When the value of α increases, the MFC state emerges from MS: Oscillators in
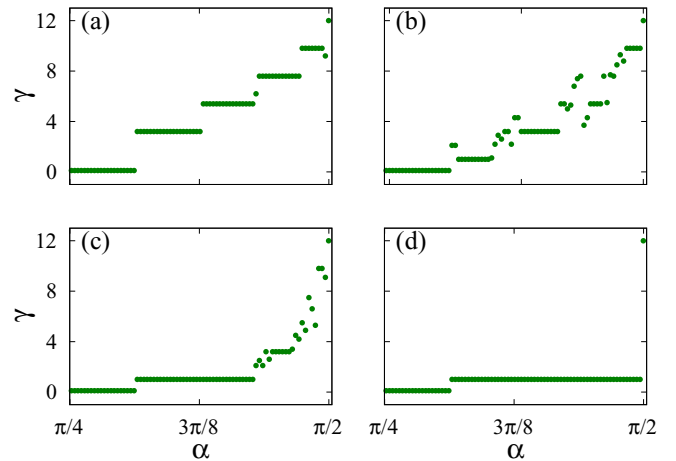

FIG. 9. The parameter γ in the network as a function of α for different values of intramodular coupling strength, (a) $\mu = 0$, (b) $\mu = 0.05$, (c) $\mu = 0.1$, and (d) $\mu = 1.0$.
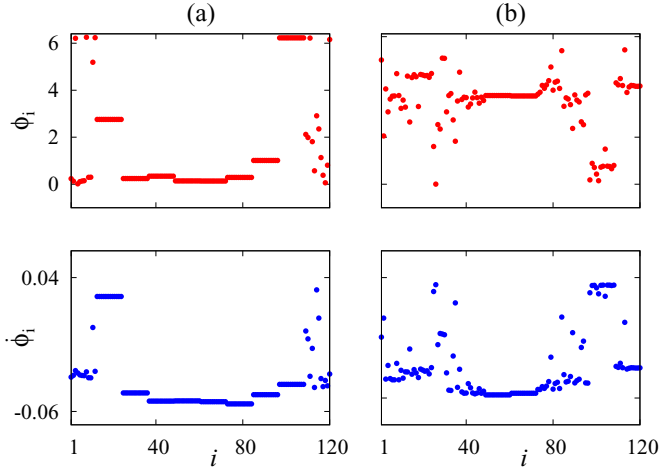
FIG. 10. Upper panel shows the phases and the lower panel the corresponding frequencies of the oscillators in the multicluster frequency chimera (MFC) state (a) $\alpha = 1.43$ on the left and (b) $\alpha = 1.55$ on the right.

some modules become desynchronized. Modules at extreme ends of the network first become desynchronized while the central modules, being the most stable, remain synchronized for a wider range of α.

An intuitive explanation for this behavior can be given in terms of the total coupling experienced by each module. There is an "edge effect" since modules at the extreme ends have a strong connection in one direction, while modules located centrally are connected strongly in both. Due to this, the modules at the extreme ends are desynchronized before the more central modules when α is increased.

Figure 10 shows the phase ϕ_i and corresponding frequency snapshots of the oscillators in a typical MFC and the dependence on α. For α close to $\pi/2$ all the oscillators in the network gradually become desynchronized.

For MS and MFC states, the frequencies of the oscillators are time dependent and the general form of the solution of Eq. (4) can be written as

$$\phi_i(t) = F_i(t) + d_i, \tag{19}$$

where F_i is a nonlinear function of time and d_i is the time-independent part. In the GS regime, by contrast, $F_i(t) = \Omega t$, and the collective frequency Ω is constant in time. This is shown in Fig. 11 where the frequencies of two randomly selected oscillators from each module are plotted. Figure 11(a) corresponds to MS, where the frequencies are time dependent and different for different modules, while Fig. 11(b) shows a MFC. For MS state, the frequencies of the oscillators within individual modules are equal but time dependent, and thus each module is separately synchronized but $\Omega^a(t) \neq \Omega^b(t)$. For other values of α when there are MFCs in the system, oscillators in some modules are synchronized with each module locked to a different (but time-dependent) frequency, while the oscillators in other modules are phase incoherent, although they all have similar time-dependent frequencies [Fig. 11(b)].

There is a symmetry in the mean frequencies of the modules: the time-averaged frequencies of modules a and
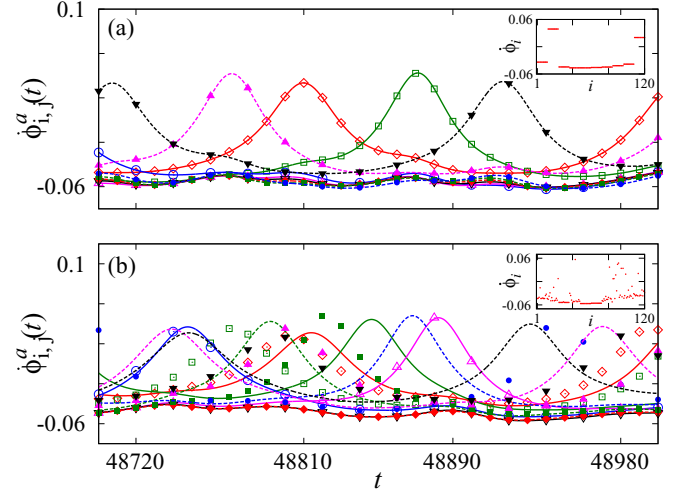
$(M + a - 1)$ are equal. This is shown in Fig. 12, where time-averaged frequencies $\langle \dot{\phi}_i(t) \rangle$ of all oscillators are plotted as a function of α at different μ values. In GS regime, time-averaged frequencies of all oscillators are equal since they all lock to the time-independent synchronized frequency Ω. However, the GS state loses stability when α is increased and the mean frequencies of the modules systematically break up pairwise with the modules at extreme ends splitting first [see Figs. 12(c) and 12(d)].

The stability of these different states can be analyzed by considering a symmetric perturbation in two arbitrary oscillators of each module [38], $\phi_{1,2}^a = \Phi^a \pm \xi^a$, where,
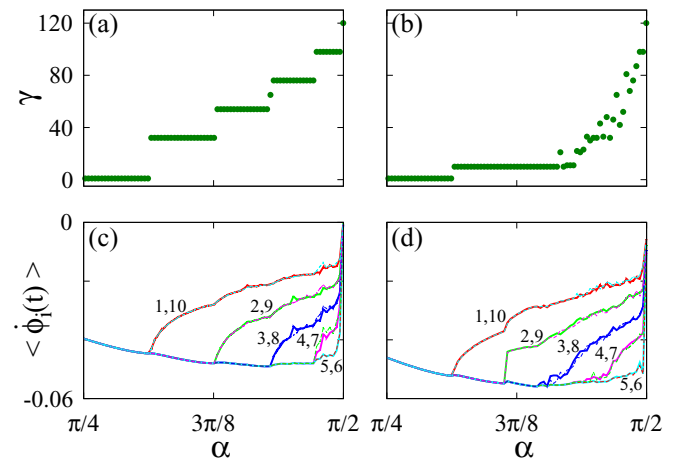

FIG. 11. For MS (a) and MFCs (b), the time-dependent frequencies $\dot{\phi}_{i,j}^a(t)$ of two arbitrarily chosen oscillators, i and j (lines and symbols respectively), are plotted from each module $a = 1, \ldots, 10$. Frequency snapshots of both states (MS and MFCs) are shown in the insets.

FIG. 12. The order parameter γ (upper panel) and the time-averaged frequencies $\langle \dot{\phi}_i(t) \rangle$ of the oscillators (lower panel) are plotted as a function of α for $\mu = 0$ (left panel) and $\mu = 0.1$ (right panel), respectively. The time-averaged frequencies of ath and $(M - a + 1)$th module are equal and when α is increased, and they systematically break pairwise as marked by index of the breaking modules.

$a = 1, \ldots, M$. In this way both the cases when individual modules are synchronized to the same frequency, namely GS, and the situation of individual modules being synchronized to different frequencies, MS, can be distinguished. The linearized variational equation for each module can be written as

$$\frac{\partial \xi^a}{\partial t} = -\frac{1}{M} \sum_{b=1}^{M} \Gamma^{ab} \cos(\Phi^b - \Phi^a - \alpha) \xi^a, \qquad (20)$$

where

$$\Gamma = \begin{bmatrix} \mu & G^{12} & G^{13} & \ldots & G^{1M} \\ G^{21} & \mu & G^{23} & \ldots & G^{2M} \\ G^{31} & G^{32} & \mu & \ldots & G^{3M} \\ \vdots & \vdots & \vdots & \ddots & \vdots \\ G^{M1} & G^{M2} & G^{M3} & \ldots & \mu \end{bmatrix}. \qquad (21)$$

Equation (20) must be solved numerically for large times along the trajectory of the entire system. When the corresponding Lyapunov exponents are calculated (one for each of the M modules), since Eq. (20) is independent of ξ^b, the corresponding Lyapunov exponents indicate the behavior of the individual module, and module desynchronization is indicated by the Lyapunov exponents crossing zero. In Fig. 13 the Lyapunov exponents λ have been plotted with the parameter γ as a function of α for two cases, $\mu = 0$ namely when the network exhibits GS and MFC but no MS and the other for $\mu = 0.1$ when all three states occur. In the GS state, all Lyapunov exponents are negative with pairs of Lyapunov exponents behaving identically, reflecting the phase symmetry observed in GS state.

The Lyapunov exponents remain negative for MS which is also a synchronized state, but when the synchronized state loses stability, one pair of Lyapunov exponents crosses zero. As the system enters into MFC more and more Lyapunov exponents cross zero, corresponding to the gradual desynchronization of successive modules. When $\mu = 0$, the modules gets desynchronized systematically and the corresponding Lyapunov exponents crosses the zero line in the systematic
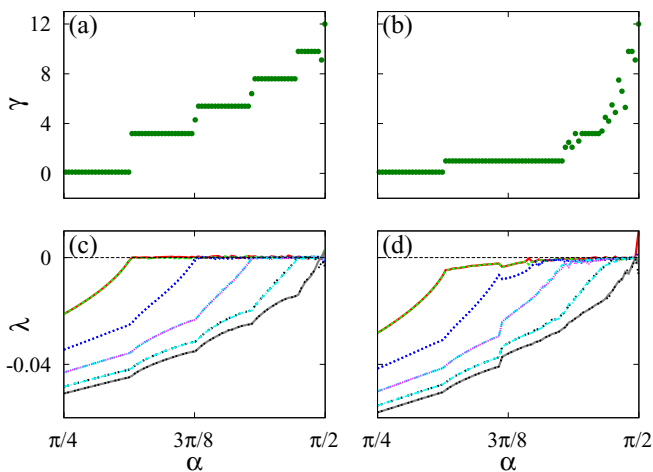
fashion as can be seen in Fig. 13. The crossings of the Lyapunov exponents therefore indicate the values of α where the transitions between the states occur.

D. Dimensional reduction

In the limit of large N the system can be reduced to a finite set of equations using the Ott and Antonsen (OA) ansatz [36]. We briefly recall some of the essential steps in the procedure here. Rewriting Eq. (1) in terms of the modules, one has

$$\frac{d\phi_i^a}{dt} = \omega + \sum_{b=1}^{M} \frac{\Gamma^{ab}}{N} \sum_{j=1}^{n} \sin\left(\phi_j^b - \phi_i^a - \alpha\right). \qquad (22)$$

In the continuum limit the dynamics of the system can be described in terms of the density function $f^a(\phi^a, t)$ that represents the density of the oscillators in module a, the corresponding phase being ϕ^a. Since the number of oscillators in each module is conserved, $f^a(\phi^a, t)$ satisfies the continuity equation,

$$\frac{\partial f^a}{\partial t} + \frac{\partial (f^a v^a)}{\partial \phi^a} = 0. \qquad (23)$$

Following OA, the velocity of the oscillators in terms of $f^a(\phi^a, t)$ can be written as

$$v^a = \omega + \sum_{b=1}^{M} \frac{\Gamma^{ab}}{M} \int_0^{2\pi} \sin(\phi^b - \phi^a - \alpha) f^b(\phi^b, t) d\phi^b. \qquad (24)$$

In order to measure the synchrony in different modules it is convenient to define the complex order parameter

$$z^a(t) = \sum_{b=1}^{M} \frac{\Gamma^{ab}}{M} \int_0^{2\pi} e^{i\phi^b} f^b(\phi^b, t) d\phi^b. \qquad (25)$$

Using this expression in Eq. (24), we get

$$v^a = \omega + \frac{1}{2i}[e^{-i\phi^a} e^{-i\alpha} z^a(t) - e^{i\phi^a} e^{i\alpha} z^{a*}(t)]. \qquad (26)$$

Now expanding $f^a(\phi^a, t)$ in a Fourier series [36],

$$f^a(\phi^a, t) = \frac{1}{2\pi} \left\{ 1 + \left[\sum_{k=1}^{\infty} (p^a(t) e^{i\phi^a})^k + \text{c.c.} \right] \right\}, \qquad (27)$$

where c.c. indicates the complex conjugate, and, substituting the expression of f^a and v^a in Eq. (23), we get

$$\frac{dp^a}{dt} = -i\omega p^a + \frac{1}{2}(p^a)^2 z^a e^{-i\alpha} + \frac{1}{2}(z^a)^* e^{i\alpha}. \qquad (28)$$

The order parameter can be written as

$$z^a(t) = \sum_{b=1}^{M} \frac{\Gamma^{ab}}{M} [p^b(t)]^*, \qquad (29)$$

while the complex variable p^a can be written in polar coordinates as
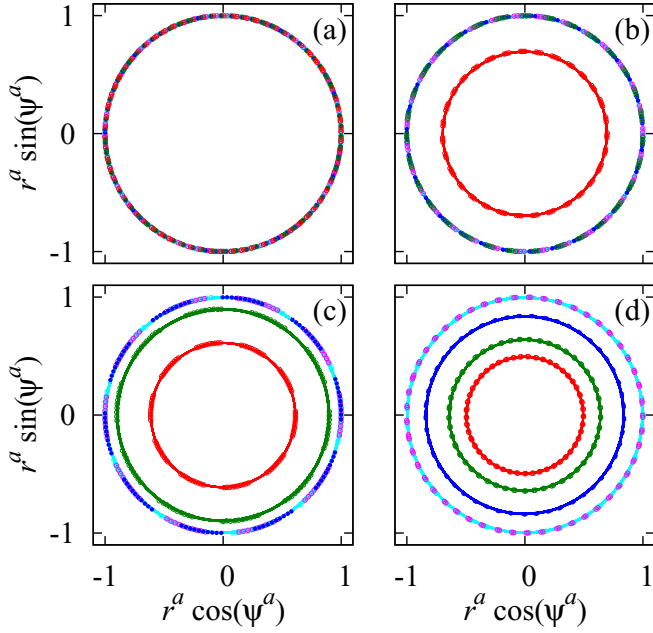
$$p^a = r^a e^{-i\psi^a}. \qquad (30)$$

FIG. 13. The parameter γ and Lyapunov exponents λ as a function of α showing crossing of Lyapunov exponents where transitions between different states occur for $\mu = 0.0$ [(a) and (c)] and $\mu = 0.1$ [(b) and (d)].

FIG. 14. System dynamics in terms of polar coordinates r^a and ψ^a for $\mu = 0$. The real and imaginary components, ($r^a \cos \psi^a$ and $r^a \sin \psi^a$, respectively) for each module are plotted for different values of α (a) $\alpha = 0.7$, (b) $\alpha = 1.1$, (c) $\alpha = 1.2$, and (d) $\alpha = 1.4$. The radius of the circle corresponds to the state of the module: $r_a = 1$ indicates the module is synchronized, whereas $r_a < 1$ for desynchronized dynamics in a module.

With a little algebra, the evolution equations for the variables r^a and ψ^a for each module are obtained as

$$\frac{dr^a}{dt} = \frac{1 - (r^a)^2}{2} \sum_{b=1}^{M} \frac{\Gamma^{ab}}{M} r^b \sin(\psi^b - \psi^a + \beta), \quad (31)$$

and

$$\frac{d\psi^a}{dt} = -\frac{1 + (r^a)^2}{2r^a} \sum_{b=1}^{M} \frac{\Gamma^{ab}}{M} r^b \cos(\psi^b - \psi^a + \beta), \quad (32)$$

where $\beta = \pi/2 - \alpha$. Thus the full system can be reduced to $2M$ equations for the components of the module order parameters, r^a and ψ^a. Note that if all the oscillators in a given module a are synchronized, then $r^a = 1$ while any value of r^a less than 1 indicates desynchrony. The global dynamics is characterized by the average $r_{\text{avg}} = \frac{1}{M} \sum_{a=1}^{M} r^a$: for both global synchrony or modular synchrony it is clear that $r_{\text{avg}} = 1$ while $r_{\text{avg}} < 1$ indicates the MFC.

The overall system behavior can be conveniently visualized by examining the dynamics of the order parameters, namely the solutions to Eqs. (31) and (32); these are shown for different α in Fig. 14. As discussed above, coherence in the dynamics of the ath module is characterized by r^a. For GS or MS, $r^a = 1$ [see Fig. 14(a) for $\alpha = 0.7$]. Upon further increasing α, the system enters into the MFC state where some modules get desynchronized. The systematic desynchronization of the modules can be seen in Figs. 14(b)–14(d), with $r^a = 1$ and $r^a < 1$ corresponding to the synchronized and desynchronized modules, respectively. The variation of r_{avg} as a function of α
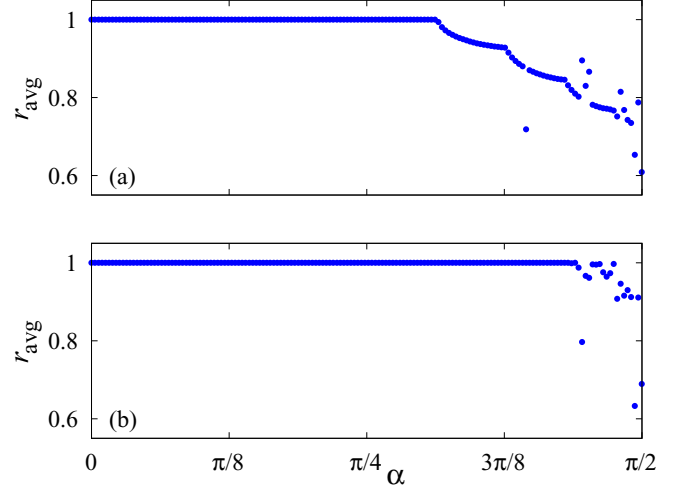

FIG. 15. Variation of the average order parameter r_{avg} as a function of the phase-lag parameter, α, for (a) $\mu = 0$ and (b) $\mu = 0.1$.

is shown for $\mu = 0$ and $\mu = 0.1$ in Fig. 15. This analysis can thus differentiate between MFC and purely synchronized dynamics.

For an ensemble of oscillators that have an intrinsic spread in the natural frequencies, the OA analysis indicates [36] that in the thermodynamic limit the dynamics is attracted to a single manifold. However, as has been pointed out by Pikovsky and Rosenblum [34] if the frequencies are all identical a more general form applies and there can be several attracting states [39]. The behavior of the reduced system, namely Eqs. (31) and (32) can then depend on initial conditions in the MFC regime and therefore also the order parameters defined above and plotted in Figs. 14 and 15.

The existence of different dynamical states can be understood in terms of the effect of three competing factors. The first one is the phase frustration parameter α which favors disorder in the system. The other two factors are intermodular nonlocal coupling and intramodular interaction μ, that support inter- and intramodular synchronization, respectively. In the absence of intramodular interactions, the increase in phase frustration parameter α destroys GS by breaking the synchronized modules systematically (due to the nonlocal nature of the coupling). However, for finite value of μ, oscillators within each module tend to synchronize even if the synchronization between the modules may not exist. This leads to the MS (for lower α values) and MFC (for higher α values) states observed in the system.

IV. SUMMARY

In the present work we have examined the manner in which nonlocal coupling affects dynamics in oscillator networks that have a modular structure. The existence of modules creates new types of chimeric states. In one case, a number of different coherent modules coexist, while in the other, some modules are coherent, while others are desynchronized. The occurrence of chimera states in the present case is due to heterogeneity in the coupling. However, the chimeras observed here differ from the phase chimeras observed by Zhu and colleagues

[40] in nonlocally coupled network of phase oscillators and partially synchronized state reported in coupled identical phase oscillators with scale-free distribution of coupling strengths [41] where all oscillators in the synchronized group lock to a single frequency.

The modular structure that we have explored here arises from a differential coupling pattern. The entire network is separated into a fixed number of modules. The intramodular coupling is controlled by one parameter, while the intermodular coupling, which is also nonlocal, is tuned by a different parameter, making it possible to examine different limits with this partitioning. We have examined the effects of changing the number of nodes in each module, as also in changing the nature of the nonlocal coupling, and find that the qualitatively results are robust.

In many experiments in neuroscience, for example, those that involve recording scalp electroencephalogram, different types of synchronization can be observed [42]. During various mental activities different neuronal networks may start to oscillate with different frequencies [43]. This is similar to modular synchronization state observed here in nonlocally coupled modular network. Similar analogy can be drawn between multicluster frequency chimeras and the so–called type 2 synchronization, where each subnetwork in the brain may oscillate synchronously, but oscillations of some specific frequencies disappear [42].

The existence of these different kinds of chimera states in networks with the modular architecture opens new avenues for further research through a systematic study of the role of network architecture and the effect of heterogeneity on such states. Clearly there are many generalizations of the topology that we have examined as well as the coupling scheme used that would be interesting to study. The effect of time delay is also important, although the phase-lag parameter can be interpreted as time delay in the coupling when delay is very small. The role of phase lag between nodes in balancing spontaneous order and permanent disorder in the network [20] has been noted in earlier work, and this parameter also offers another avenue for exploring the dynamics of modular networks.

ACKNOWLEDGMENTS

[1] S. H. Strogatz, D. M. Abrams, A. McRobie, B. Eckhardt, and E. Ott, Nat. Phys. **438**, 43 (2005).

[2] Y. Kuramoto, *Chemical Oscillations, Waves and Turbulence* (Springer-Verlag, Berlin, 1984).

[3] M. Wickramasinghe and I. Z. Kiss, PLoS ONE **8**, e80586 (2013).

[4] M. Toiya, H. Gonzalez-Ochoa, V. K. Vanag, S. Fraden, and I. R. Epstein, J. Phys. Chem. Lett. **1**, 1241 (2010).

[5] A. T. Winfree, *The Geometry of Biological Time* (Springer, New York, 1980).

[6] M. Girvan and M. E. J. Newman, Proc. Natl. Acad Sci. USA **99**, 7821 (2002).

[7] A. Arenas, A. Díaz-Guilera, J. Kurths, Y. Moreno, and C. Zhou, Phys. Rep. **469**, 93 (2008).

[8] E. Oh, K. Rho, H. Hong, and B. Kahng, Phys. Rev. E **72**, 047101 (2005); A. Arenas, A. Díaz-Guilera, and C. J. Pérez-Vicente, Phys. Rev. Lett. **96**, 114102 (2006).

[9] A. Pikovsky, M. Rosenblum, and J. Kurths, *Synchronization—A Universal Concept in Nonlinear Sciences* (Cambridge University Press, Cambridge, 2001).

[10] S. H. Strogatz, Nat. Phys. **410**, 268 (2001).

[11] K. Kaneko and I. Tsuda, *Chaos and Beyond, A Constructive Approach with Applications in Life Sciences* (Springer, Berlin, 1996).

[12] J. A. Acebron, L. L. Bonilla, C. J. P. Vicente, F. Ritort, and R. Spigler, Rev. Mod. Phys. **77**, 137 (2005).

[13] N. Go and H. Taketomi, Proc. Natl. Acad Sci. USA **75**, 559 (1978).

[14] H. Sakaguchi, Phys. Rev. E **73**, 031907 (2006).

[15] B. Ermentrout, Rep. Prog. Phys. **61**, 353 (1998).

[16] H. Kori and A. S. Mikhailov, Phys. Rev. Lett. **93**, 254101 (2004); Phys. Rev. E **74**, 066115 (2006).

[17] Y. Kuramoto and D. Battogtokh, Nonlinear Phenom. Complex Syst. (Minsk, Belarus) **5**, 380 (2002).

[18] D. M. Abrams and S. H. Strogatz, Phys. Rev. Lett. **93**, 174102 (2004).

[19] G. C. Sethia and A. Sen, Phys. Rev. Lett. **112**, 144101 (2014).

[20] M. J. Panaggio and D. M. Abrams, Nonlinearity **28**, R67 (2015).

[21] N. C. Rattenborg, C. J. Amlaner, and S. L. Lima, Neurosci. Biobehav. Rev. **24**, 817 (2000).

[22] C. R. Laing and C. C. Chow, Neural Comput. **13**, 1473 (2001); C. R. Laing, W. C. Troy, B. Gutkin, and G. B. Ermentrout, SIAM J. Appl. Math. **63**, 62 (2002).

[23] A. E. Motter, S. A. Myers, M. Anghel, and T. Nishikawa, Nat. Phys. **9**, 191 (2013).

[24] F. Dörfler, M. Chertkov, and F. Bullo, Proc. Natl. Acad Sci. USA **110**, 2005 (2013).

[25] M. R. Tinsley, S. Nkomo, and K. Showalter, Nat. Phys. **8**, 662 (2012); A. M. Hagerstrom, T. E. Murphy, R. Roy, P. Hövel, I. Omelchenko, and E. Schöll, *ibid.* **8**, 658 (2012).

[26] E. A. Martens, C. R. Laing, and S. H. Strogatz Phys. Rev. Lett. **104**, 044101 (2010); E. A. Martens, S. Thutupalli, A. Fourriére, and O. Hallatschek, Proc. Natl. Acad Sci. USA **110**, 10563 (2013).

[27] A. E. Motter, Nat. Phys. **6**, 164 (2010).

[28] L. Larger, B. Penkovsky, and Y. L. Maistrenko, Phys. Rev. Lett. **111**, 054103 (2013).

[29] C. R. Laing, K. Rajendran, and I. G. Kevrekidis, Chaos **22**, 013132 (2012); C. R. Laing, Phys. Rev. E **81**, 066221 (2010); Physica D **238**, 1569 (2009).

[30] Y. Kawamura, Phys. Rev. E **75**, 056204 (2007).

[31] G. C. Sethia, A. Sen, and F. M. Atay, Phys. Rev. Lett. **100**, 144102 (2008); J. H. Sheeba, V. K. Chandrasekar, and M. Lakshmanan, Phys. Rev. E **79**, 055203(R) (2009).

[32] I. Omelchenko, Y. Maistrenko, P. Hovel, and E. Schöll, Phys. Rev. Lett. **106**, 234102 (2011).

[33] S. R. Ujjwal and R. Ramaswamy, Phys. Rev. E **88**, 032902 (2013).

[34] A. Pikovsky and M. Rosenblum, Phys. Rev. Lett. **101**, 264103 (2008).

[35] M. Shanahan, Chaos **20**, 013108 (2010); M. Wildie and M. Shanahan, *ibid.* **22**, 043131 (2012).

[36] E. Ott and T. M. Antonsen, Chaos **18**, 037113 (2008); **19**, 023117 (2009).

[37] K. Premalatha, V. K. Chandrasekar, M. Senthilvelan, and M. Lakshmanan, Phys. Rev. E **91**, 052915 (2015).

[38] A. Yeldesbay, A. Pikovsky, and M. Rosenblum, Phys. Rev. Lett. **112**, 144103 (2014).

[39] E. A. Martens, Phys. Rev. E **82**, 016216 (2010).

[40] Y. Zhu, Z. Zheng, and J. Yang, Phys. Rev. E **89**, 022914 (2014).

[41] T. W. Ko and G. B. Ermentrout, Phys. Rev. E **78**, 016203 (2008).

[42] W. Klimesch, Int. J. Psychophysiol. **24**, 61 (1996).

[43] J. H. Williams, Neuroscience **104**, 283 (2001).